The LINC complex transmits integrin-dependent tension to the nuclear lamina and represses epidermal differentiation

Emma Carley[1]*, Rachel M. Stewart[1*+], Abigail Zieman[2]*, Amanda Zubek[3], Samantha Lin[2], Valerie Horsley[2,3,+], and Megan C. King[1,2,+]

[1] Department of Cell Biology, Yale School of Medicine
[2] Department of Molecular, Cell and Developmental Biology, Yale University
[3] Department of Dermatology, Yale School of Medicine

* These authors contributed equally to this work

[+] Co-corresponding authors: valerie.horsley@yale.edu or megan.king@yale.edu

Abstract:
Cell fate decisions are essential for tissue development and homeostasis and can be induced by chemical and mechanical inputs. While the mechanisms by which chemical signals control cell fate have been well studied, how mechanical inputs impact cell fate decisions are not well understood. Here, we use the well-defined system of keratinocyte differentiation in the skin to define mechanisms by which mechanical inputs control cell fate. Although mechanical signals are known to induce epidermal differentiation, whether and how direct force transmission to the nucleus regulates cell fate decisions remains unknown. Here, we measure tension on the nucleus through the Linker of Nucleoskeleton and Cytoskeleton (LINC) complexes using a molecular biosensor during keratinocyte differentiation. We show that undifferentiated epidermal stem cells display high tension on the LINC complex when integrins are engaged. During differentiation, tension decreases on the LINC complex and on A-type lamins, suggesting that the state of the nuclear lamina is altered during differentiation. LINC complex ablation in mice reveals that LINC complexes are required to repress epidermal differentiation *in vitro* and *in vivo*, suggesting that force transduction from engaged integrins to the nucleus plays a role in maintaining keratinocyte progenitors. This work reveals a direct mechanotransduction pathway capable of relaying adhesion-specific signals to regulate cell fate.

Introduction:

Physical forces and the architecture of the extracellular environment are an emerging area of cell fate regulation (Discher et al., 2009). Cells sense changes in physical environment through cell-cell and cell-extracellular matrix (ECM) adhesions and these mechanical inputs can control cell fate. While several studies have linked geometrical and physical inputs to changes in cellular signaling through the transcription factors, YAP/TAZ (Totaro et al., 2018) or nuclear localization of the activator of serum response factor, MKL/MRTF (Connelly et al., 2010), whether direct transmission of mechanical force to the nucleus can influence cell fate is not known.

The interfollicular epidermis is an excellent model to explore how mechanical inputs regulate cell fate. Epidermal stem cells adhere to the underlying basal lamina through β1 integrin-based adhesions and β4 integrin-based hemidesmosomes (Raghavan et al., 2000), which maintain stem cell fate, proliferation, and inhibit differentiation (Hotchin et al., 1995; Levy et al., 2000; Rippa et al., 2013; Watt et al., 1993). Upon differentiation, basal keratinocytes release their integrin-based adhesions, initiate gene expression changes to activate terminal differentiation (Tsuruta et al., 2011), and move upward to enter the stratified epithelium until they are shed at the skin's surface. Despite the well-established role for integrin adhesions in regulating epidermal differentiation, how integrin signals are propagated to the nucleus to regulate the keratinocyte differentiation program is not well understood.

Here, we explore whether mechanical cues can regulate keratinocyte cell fate via tension on the nucleus via the Linker of Nucleoskeleton and Cytoskeleton (LINC) complex. The LINC complex, composed of tail-anchored Nesprins integrated into the outer nuclear membrane and SUN proteins integrated into the inner nuclear membrane, spans the nuclear envelope to mechanically integrate the cytoplasmic cytoskeleton and the nuclear interior – specifically the nuclear lamina and its associated chromatin (Chang et al., 2015). While the LINC complex has been postulated to act either as a direct mechanosensor or as a conduit for mechanotransduction, to influence gene expression (Alam et al., 2016; Wang et al., 2009), whether the LINC complex controls gene expression *in vivo* remains largely untested. Indeed, to date direct gene targets of the LINC complex that regulate genetic programs *in vivo*, for example during differentiation, remain to be identified.

Several lines of evidence suggest that epidermal differentiation is regulated by the nuclear lamina, yet the mechanisms remain unknown. First, during basal stem cell differentiation, a large chromosomal region termed the epidermal differentiation complex (EDC), which consists of sixty consecutive genes necessary for epidermal stratification and the production of the cornified envelope, relocates away from the nuclear lamina towards the nuclear interior to be transcriptionally activated (Gdula et al., 2013; Mardaryev et al., 2014; Williams et al., 2002)). Further, the AP-1 transcription factor complex, itself regulated by A-type lamins, influences EDC gene expression in both proliferating and differentiating keratinocytes *in vitro* (Oh et al., 2014) and coordinates with EZH2 in the polycomb complex to regulate epidermal differentiation (Ezhkova et al., 2009). Lastly, a skin-specific lamin-null mouse model (Lamin B1/B2/A/C triple-knockout) exhibits a thickened epidermis attributed to precocious differentiation (Jung et al., 2014).

Here, we provide evidence that the LINC complex regulates epidermal differentiation *in vitro* and *in vivo*. Using a novel molecular biosensor to measure forces exerted on LINC complex molecules, we find that tension is high on the LINC complex and A-type lamins in epidermal stem cells in an integrin dependent manner and is reduced upon differentiation. In mouse keratinocytes lacking LINC complexes we observe precocious differentiation *in vitro* and expansion of the differentiated, suprabasal layers of the skin *in vivo*. This work suggests that tension from integrins

is communicated through the LINC complex to the nuclear lamina to maintain the progenitor state of basal keratinocytes, providing a potential mechanism by which cell fate is regulated directly by mechanical cues.

Results and Discussion:

A tension sensor in Nesprin-2 is sensitive to integrin engagement

In order to visualize tension on the LINC complex in living cells, we generated a molecular biosensor to measure tension on individual Nesprin proteins. To this end, we inserted a tension sensor module composed of the fluorescence resonance energy transfer (FRET) pair mTFP and Venus connected by an elastic flagelliform linker (Grashoff et al., 2010) into the juxtamembrane region of a mini-Nesprin-2 construct [REF- Gant], called hereafter "N2G-JM-TSMod". This TSMod has been shown previously to be sensitive to forces in the single pN range [REF Schwartz]. In this construct, the TSMod lies between the transmembrane domain and the entire cytosolic domain of Nesprin-2, which contains both the N-terminal calponin homology domains that engage actin and the spectrin repeat region (**Fig. 1A**). This strategy will allow binding to actin and engagement with SUN proteins at the nuclear envelope through the C-terminal KASH domain, making it distinct from a previously-described tension sensor [REF Hoffman]. Furthermore, when the N2G-JM-TSMod is relaxed, the FRET ratio is high, while tension will lead to a decrease in the FRET ratio (**Fig. 1A**).

To measure LINC complex tension, we expressed the N2G-JM-TSMod in primary undifferentiated mouse keratinocytes (MKCs). The N2G-JM-TSMod targeted efficiently to the nuclear envelope in MKCs when expressed at moderate levels (**Fig. 1B**). To determine if integrin adhesions altered tension on the LINC complex, we plated MKCs expressing N2G-JM-TSMod on glass coverslips coated with fibronectin, which will engage integrins, or on poly-L-lysine, which will not engage integrin adhesions. MKCs that were fully spread (after 24 hrs) on fibronectin-coated glass surfaces displayed lower N2G-JM-TSMod FRET ratios (higher tension) than MKCs fully spread instead on poly-L-lysine (**Fig. 1B** and **Fig. 1C**). We also noted that LINC complex tension was lower in MKCs that were not fully spread on fibronectin substrates (after 4 hrs) compared to fully spread MKCs. Thus, engagement of integrins with fibronectin (through focal adhesions) is important for a high-tension state on the N2G-JM-TSMod.

Since the actin network engages integrin adhesions, we analyzed whether actin was required for tension on N2G-JM-TSMod in undifferentiated MKCs. We plated MKCs on fibronectin for 24 hrs and then pharmacologically disrupted filamentous actin with latrunculin. Indeed, after 5 hours of latrunculin treatment, the N2G-JM-TSMod displayed relaxed tension compared to the vehicle control (**Fig. 1C**). Taken together, high tension on the N2G-JM-TSMod in undifferentiated MKCs requires both integrin engagement and filamentous actin.

Cell-intrinsic integrin engagement predicts N2G-JM-TSMod tension and differentiation in cohesive MKC colonies

Primary MKCs can be induced to differentiate *in vitro* by elevating extracellular calcium levels, leading to the formation of cohesive colonies that engage E-cadherin-based cell-cell adhesions and subsequently differentiate as assessed by up-regulation of markers expressed in epidermal suprabasal layers *in vivo*. In our previous work, we demonstrated that this transition leads to a reorganization of focal adhesions and traction stresses to cells at the colony periphery, while cells in the colony interior solely engage cell-cell adhesions (Mertz et al., 2013)(**Fig. 2A**). To test if tension on the N2G-JM-TSMod is sensitive to the presence of cell intrinsic focal adhesion engagement, we segmented cells in cohesive MKC colonies into "periphery" and "interior" cells. We find that the FRET ratio of the N2G-JM-TSMod for interior cells is significantly higher than that observed for cells at the colony periphery (**Fig. 2B**), indicating that tension on the LINC complex is lost in interior cells that contain solely cell-cell adhesions. These data are consistent with the ability of fibronectin-based focal adhesions to drive LINC complex tension in a cell intrinsic manner in undifferentiated MKCs.

Given that the LINC complex has been shown to transmit tension from the cell substrate to the lamin network at the nuclear periphery [Ihalalein], we examined whether tension on lamin A/C within cohesive MKC colonies mirrored that observed for the LINC complex with the N2G-JM-TSMod. To this end, we employed a conformationally sensitive lamin A/C antibody, which has been used to examine changes in lamin tension due to substrate stiffness (Ihalainen et al., 2015). When lamins are under tension, the epitope of lamin A/C becomes inaccessible, resulting a decrease in fluorescence. We immunostained differentiated mouse keratinocyte colonies with a conformationally sensitive lamin A/C antibody and examined cells at the periphery and interior. We imaged nuclei in which the apical and basal nuclear membranes were distinct and quantified the fluorescent signal in the z-plane as in (Ihalainen et al., 2015). We fitted the signal with two gaussian curves and extracted the ratio of the basal to apical intensity (**Fig. 2C**) across many colonies (n=17). In cells at the colony periphery, we observe a strong bias of fluorescence at the apical nuclear surface compared to the basal surface (**Fig. 2D**), indicating that tension on the lamin network is high on the basal surface in cells at the periphery of colonies. By contrast, cells in the colony interior display far more uniform conformationally sensitive lamin A/C staining (**Fig. 2C**), indicating that tension on the lamin network is reduced in cells in the colony interior. Taken together, these results suggest that cells at the colony periphery that engage focal adhesions have high tension on both LINC complexes and the nuclear lamina, while cells at the colony interior possess relaxed LINC complexes and lamin A/C.

To examine whether the cells in the colony interior are more differentiated, we performed RNA fluorescence in-situ hybridization (FISH) for *Sprr1b* mRNA, which is upregulated in differentiated MKCs and is found in the EDC. We find that MKCs at the colony interior express more *Sprr1b* mRNA 24 and 48 hours after induction of differentiation compared to cells at the colony periphery (**Fig. 2E-F**). We made similar observations for expression of involucrin (**Fig. 2-figure supplement 1**). Taken together, these results indicate that tension on LINC complexes and the nuclear lamina is more prominent in cells that maintain integrin adhesions and a progenitor fate.

The epidermis of *Sun* dKO mice displays precocious differentiation despite normal adhesion To determine whether tension on LINC complexes controls MKC differentiation, we analyzed the skin of mouse models lacking the ubiquitously expressed SUN proteins, SUN1 and SUN2, which are expected to lack all LINC complexes in somatic tissues [Han papers]. Although *Sun1*$^{-/-}$/*Sun2*$^{-/-}$ (hereafter *Sun* dKO) mice die after birth (Zhang et al., 2009), we were able to analyze the developing epidermis of *Sun* dKO mice prior to birth. Western blot analysis revealed that SUN1 and SUN2 proteins were absent in the skin of *Sun* dKO compared to WT mice that express both SUN proteins (**Fig. 3-figure supplement 1**).

At E15.5 histological analysis of skin tissue revealed a thickening of the epidermis in the *Sun* dKO mouse compared to WT littermates (**Fig. 3A**). Immunostaining of skin sections of WT and *Sun* dKO mice with antibodies against keratin-10 (K10), a marker of the differentiated spinous layer of the epidermis, revealed an expansion of the spinous layer of the *Sun* dKO epidermis (**Fig. 3B** and **3C**). To further examine whether the thickened epidermis of *Sun* dKO mice resulted from changes in differentiation and/or proliferation, we performed an EdU pulse chase experiment. We labelled proliferating basal progenitor keratinocytes in embryonic WT and *Sun* dKO mice with EdU and examined the skin after 24 hrs (**Fig. 3D**). Immunostaining skin sections with K10 antibodies and staining for EdU incorporation revealed that the total number of EdU-positive cells was similar between WT and *Sun* dKO epidermis, indicating that basal cell proliferation was not altered in the absence of LINC complexes in skin (**Fig. 3E**). However, while EdU-positive cells were restricted to the basal, K10-negative layer in WT tissue (**Fig. 3F**), EdU-positive cells were observed in both the basal layer as well as the suprabasal, K10-positive layers in *Sun* dKO skin (**Fig. 3D** and **3F**).

These results indicate that *Sun* dKO keratinocytes precociously differentiate *in vivo* without changes in proliferation.

As integrin signals are required to repress the differentiation of basal keratinocytes, we explored the possibility that cell-matrix adhesions are altered in number and/or size in the epidermis of *Sun* dKO mice. We therefore performed electron microscopy on skin sections from heterozygous (*Sun1/2+/-*) and *Sun* dKO mice at P0.5. The basal layer-basal lamina interface in *Sun1/2+/-* and *Sun* dKO skin appeared indistinguishable, displaying tight association in mice from both genotypes (**Fig. 3G**). Moreover, hemidesmosomes (which can be observed in electron micrographs, arrows) were of equivalent number and size (**Fig. 3H**). These observations suggest that *Sun* dKO mice display precocious epidermal differentiation in vivo that is uncoupled from changes in adhesion between basal keratinocytes and the basal lamina.

Sun* dKO MKCs exhibit precocious differentiation *in vitro

To further analyze keratinocyte differentiation, we isolated WT and *Sun* dKO MKCs from newborn mice and performed global transcriptional profiling on WT and *Sun* dKO MKCs grown in either low calcium media to maintain a progenitor state or high calcium media to induce differentiation. Gene ontology analysis revealed striking differences in the expression of genes associated with keratinocyte differentiation between WT and *Sun* dKO MKCs in both low and high calcium, including those that reside in the EDC (**Fig. 4A-B**). Further examination of these RNAseq data revealed evidence of precocious differentiation in *Sun* dKO MKCs. For example, numerous members of the gene family in the SPRR region of the EDC (**Fig. 4**) were de-repressed in *Sun* dKO MKCs grown in the low calcium condition (**Fig. 4C**). We validated this global analysis by RT-qPCR analysis of *Sprr* genes (**Fig. 4D** and **Fig. 4-figure supplement 1).** Not only do we observe precocious expression of genes such as *Sprr1b* in *Sun* dKO MKCs cultured in low calcium media, but we also observe much higher expression in the presence of calcium in *Sun* dKO MKCs (**Fig. 4D** and **Fig. SX**). RNA FISH analysis of the *Sprr1b* (**Fig. 3E**) and *Ivl1* (**Fig. 4-figure supplement 1**) transcripts further confirmed that *Sun* dKO MKCs displayed higher expression levels of differentiation genes compared to WT MKCs.

Since we found that the differentiated, interior MKCs within cohesive colonies displayed low tension on the LINC complex and A-type lamins (**Fig. 2**), we hypothesized that the lack of LINC complexes may result in differentiation of progenitor cells at the colony periphery. To address this hypothesis, we performed RNA FISH on WT and *Sun* dKO MKCs. While WT MKCs biased expression of differentiation markers such as *Sprr1b* and *Ivl* at the colony interior over the colony periphery (**Fig. 2F**), *Sun* dKO MKC colonies expressed *Sprr1b* mRNAs in both interior and cells at the colony periphery (**Fig. 4F, arrows**), despite still having focal adhesions in peripheral cells (**Fig. 4-figure supplement 2**). As a consequence, expression of differentiation markers is random with respect to colony position in the absence of LINC complexes (**Fig. 4G**). Taken together, these results suggest that LINC complexes are required to repress epidermal differentiation genes when integrins are actively engaged.

Discussion:

Here we demonstrate that LINC complex tension in MKCs responds specifically to integrin-engagement in a cell-intrinsic manner. While integrin-dependent signals normally repress the differentiation of keratinocytes, in the absence of functional LINC complexes these basal progenitors instead differentiate precociously both *in vitro* and *in vivo*. While it is tempting to speculate that LINC complexes transmit forces from the integrin-engaged actin network to the nuclear lamina to directly regulate the expression of epidermal differentiation genes, we cannot yet rule out the alternative possibility that loss of the LINC complex indirectly affects an alternative signaling pathway. However, as our electron microscopy data strongly suggest that adhesion between basal keratinocytes and the basal lamina remains normal in *Sun* dKO animals, we favor this direct model (**Fig. 5**).

How might tension on the nuclear lamina regulate epidermal differentiation? As a skin-specific mouse model lacking A- and B-type lamin expression also demonstrated precocious epidermal differentiation (Jung et al., 2014) and we find that MKC differentiation coincides with a relaxation of lamin A/C tension (**Fig. 2C-D**), one attractive model is that the LINC complex acts through tension-dependent remodeling of the nuclear lamina. The chromosome region housing the EDC moves away from the nuclear lamina during epidermal differentiation (Gdula et al., 2013; Mardaryev et al., 2014; Williams et al., 2002) and is associated with the loss of H3K27me3 chromatin marks on differentiation-specific genes (Lien et al., 2011). If and how lamin tension influences this change in nuclear compartmentalization remains to be defined. We favor a model in which stretching of lamins drives remodeling of the composition of the nuclear lamina to maintain the epidermal progenitor state. Interestingly, the conformational epitope in lamin A/C examined in this work (**Fig. 2**) overlaps with binding sites for DNA, histones, SUN proteins, and the integral inner nuclear membrane protein emerin (Ihalainen et al., 2015). Thus, the force-dependent differential exposure of these binding sites may influence the interaction of lamin A/C with the genome, either directly or through modulation of the activity of its binding partners. Indeed, stretching of MKCs leads to the release of emerin from the nuclear lamina; abrogating this mechanical response also leads to precocious differentiation (Le et al., 2016). Moreover, this response involves the formation of a perinuclear actin cage, a structure which we found previously to be perturbed in MKCs lacking SUN2 (Stewart et al., 2015).

Further work will be required to determine if the levels and geometry of forces exerted on LINC complexes differ between integrin-based adhesions and cell-cell adhesions. Examining whether the geometry of exogenous force application to cells influences nuclear lamina-dependent regulation of gene expression by modulating the extent of chromatin stretch (Tajik et al., 2016) represents another exciting direction.

Materials and Methods

Cell culture and plasmid transfection

Mouse keratinocytes were isolated from skin from E18.5 embryos or newborn *Sun1*$^{-/-}$/*Sun2*$^{-/-}$ or WT pups as previously described (Mertz et al., 2013). Under sterile conditions, pups were sacrificed, and back skin was excised, washed in PBS, and floated on dispase at 4°C for 16–20 h. The epidermis was separated from the dermis with forceps and incubated in 0.25% trypsin for 15 min at RT. Cells were liberated by trituration, filtered using a 40–70-µm strainer, and plated on mitomycin-C–treated J2 fibroblasts in medium-calcium medium (0.3 mM $CaCl_2$). After two to four passages, keratinocytes were plated on plastic dishes without feeder cells and maintained in media containing 0.05 mM $CaCl_2$ (E-low calcium media). Cells at low passage were stored under liquid nitrogen, and thawed cells were only used to passage 16.

Construction and application of N2G-JM-TSMod constructs

The N2G-JM-TSMod construct was derived from pEGFP-C1 harboring mini-Nesprin2 (Luxton et al., 2011)(kind gift from Gant Luxton and Gregg Gundersen). The GFP was removed by QuikChange mutagenesis. The mTFP-Venus tension sensor module (Grashoff et al., 2010) (kind gift from Martin Schwartz) was inserted just prior to the transmembrane domain. For FRET experiments, cells were plated in E-low calcium media 16 hours before transfections on glass-bottomed dishes (MatTek Corporation) coated with 50ug/ml fibronectin (20 minutes at room temperature, Sigma-Aldrich). Cells were transfected using Jetprime reagent (Polyplus) according to the manufacturer's instructions, and imaged the following day. Donor bleed-through samples consisted of cells transfected with mini-Nesprin2G-mTFP1 alone. Acceptor cross-excitation samples consisted of cells transfected with mini-Nesprin2G-Venus alone. FRET samples consisted of Nesprin2G-JM-TSMod. Actin depolymerization was achieved by the addition of 0.5µM latrunculin A (or DMSO control) for 5 hours prior to imaging.

RNA FISH experiments

WT and *Sun* dKO MKCs were plated at low density (15,000 cells/well of 24 well dish) onto glass coverslips coated with 50 µg/ml fibronectin (Sigma Aldrich), MKCs were cultured in E-low calcium media overnight before switching to 1.2 mM calcium media to induce differentiation for 24 or 48 hours. RNA FISH was performed using the ViewRNA ISH Cell Assay kit (ThermoFisher Cat# QVC0001) with probes for Involucrin (ThermoFisher Cat# VB1-3030396-VC) and Sprr1b (ThermoFisher Cat# VB4-3117172-VC) according to manufacturer's instructions. Coverslips were mounted onto glass slides with Prolong Gold with DAPI (Invitrogen P36935) and sealed with clear nail polish. Images were acquired with the Zeiss Imager M1 using Zen software. Images for the same marker were acquired at the same exposure, pixel range, and gamma values. Acquired images were equally brightened, contrasted and cropped using ImageJ National Institutes of Health (NIH; version 1.50e) software. For quantitation, signal threshold was determined using no probe controls for each individual experiment. Threshold was adjusted using ImageJ/Figi version 1.50e software from NIH. Colony outlines were drawn and then cells were counted and scored as positive or negative for gene expression and interior or periphery based on location within colony. Statistical analysis was performed using Prism 8 software.

Mouse tissue isolation, histology and immunofluorescence staining

At harvest, embryos were submerged in O.C.T compound (Tissue-Tek) and sectioned using a cryostat (CM3050S; Leica). Sections were cut in a specific and consistent orientation relative to

embryo morphology and stained with hematoxylin and eosin for routine histopathology or incubated with primary antibodies and Alexa Fluor-conjugated secondary antibodies for indirect immunofluorescence as previously described (REF: Stewart 2015). Primary antibody to keratin 10 (K10) was a gift from the Segre lab (REF). Images were acquired with the Zeiss Imager M1 using Zen software. Images for the same marker were acquired at the same exposure, pixel range, and gamma values. Acquired images were equally brightened, contrasted and cropped using ImageJ National Institutes of Health (NIH; version 1.50e) software. Spinous layer thickness was quantitated by making 5-8 measurements per image using ImageJ software. Statistical analysis was performed using Prism 8 software.

Western Blot Analysis

Whole-cell lysates of WT, *Sun2-/-*, and *Sun* dKO MKCs were prepped as previously described (Stewart et al., 2015). Primary antibodies against SUN1 (1:100, Abcam, ab124770) SUN2 (1:100; Abcam ab124916), and β-Actin (1:1,000; mouse; Abcam) were used.

EdU incorporation and quantitation

Pregnant females were pulsed with EdU via IP injection when embryos were age E14.5. 24 hours after injection, embryos were isolated and embedded in O.C.T. media (Tissue Tek) and stored at -80° C until sectioning using a cryostat (CM3050S; Leica). After sectioning, the Click-iT EdU Cell Proliferation Kit for Imaging, Alexa Fluor 488 dye (Invitrogen C10337) was used according to manufacturer's instructions to evaluate EdU incorporation. Tissue sections were then co-stained for K10 (see mouse tissue isolation, histology, and immunofluorescence staining). Before imaging, coverglass was mounted onto slides using Prolong Gold with DAPI (Invitrogen P36935) and sealed with clear nail polish. Images were acquired with the Zeiss Imager M1 using Zen software. Total Edu positive cells were counted and normalized to the total number of epidermal cells (determined by DAPI staining). Location of proliferating cells was determined by K10 staining (basal keratinocytes (EdU+/K10-), suprabasal keratinocytes (EdU+/K10+)) and then normalized to total EdU positive cells. Statistical analysis was performed using Prism 8 software.

Electron Microscopy

Transmission electron microscopy was performed in the Yale School of Medicine Center for Cellular and Molecular Imaging Electron Microscopy core facility. Back skin sections from *Sun 1+/-/Sun2-/-* and *Sun* dKO pups was isolated at age P0.5; three mice were examined for each genotype. Tissue blocks were fixed in 2.5% glutaraldehyde/2% paraformaldehyde in 0.1 M sodium cacodylate buffer, pH 7.4, for 30 min at RT and 1.5 h at 4°C. The samples were rinsed in sodium cacodylate buffer and were postfixed in 1% osmium tetroxide for 1 h. The samples were rinsed and en bloc stained in aqueous 2% uranyl acetate for 1 h followed by rinsing, dehydrating in an ethanol series to 100%, rinsing in 100% propylene oxide, infiltrating with EMbed 812 (Electron Microscopy Sciences) resin, and baking overnight at 60°C. Hardened blocks were cut using an ultramicrotome (UltraCut UC7; Leica). Ultrathin 60-nm sections were collected and stained using 2% uranyl acetate and lead citrate for transmission microscopy. Carbon-coated grids were viewed on a transmission electron microscope (Tecnai BioTWIN; FEI) at 80 kV. Images were taken using a CCD camera (Morada; Olympus) and iTEM (Olympus) software. The length and number of hemidesmosomes was quantitated from sections from 3 mice of each genotype.

Immunofluorescence

WT and *Sun* dKO keratinocytes were plated at low density (15,000 cells/well of 24 well dish) onto glass coverslips coated with 50 µg/ml fibronectin (Sigma Aldrich), MKCs were cultured in E-low calcium media overnight before switching to 1.2 mM calcium media to induce differentiation for 48 hours. Cells were fixed with methanol at -20C for 5 minutes and washed with PBS. Cells were permeabilized using 0.5% Triton X-100 in PBS at RT for 20 minutes and blocked using 10% goat serum, 5% BSA, and 0.5% Tween 20 in PBS for 1 hour. Cells were incubated in primary antibody, conformationally sensitive LaminA/C (1:200; ab8984; Abcam), diluted in blocking buffer at 4C overnight. Coverslips were washed with PBS for three 5 minute intervals and incubated with AlexaFluor 488 conjugated secondary antibody (1:1000; Invitrogen Cat# A-11029) diluted in blocking buffer at RT for 1 hour. Coverslips were then costained with Hoechst 33342 (1:2000; ThermoFisher Scientific) and Alexa Fluor 594-conjugated Wheat Germ Agglutinin (1:1000; Life Technologies) diluted in PBS for 5 minutes at RT. Coverslips were washed with PBS, mounted using Fluoromount-G and sealed with clear nail polish.

Imaging and image analysis

Live FRET imaging was performed on a Zeiss LSM 710 DUO NLO confocal microscope using a 100x, 1.4 NA oil objective with a stage maintained at 37°C and 7.5% CO_2. Images were acquired using Zen software (check this). FRET imaging was performed in a similar manner as previously described (Grashoff et al. 2010; Kumar…Schwartz, 2016 JCB). Three sequential images were acquired: the donor mTFP1 channel using a 458 nm laser line (ex), 458 nm MBS filter, and PMT detector set for mTFP1 emission; the acceptor Venus channel using a 514 nm laser line (ex), 458/514 nm MBS filter, and PMT detector set for Venus emission; and the FRET channel using a 458 nm laser line (ex), 458/514 nm MBS filter, and PMT detector set for Venus emission. In all cases, the nuclear midplane was imaged. Acquisition settings were standardized and maintained during experiments. FRET image analysis was performed using the intensity-based FRET method, implemented as previously described (Kumar, et al. 2016 JCB). Non-linear spectral bleed-through corrections were first determined using the PixFRET plugin (Feige…Gelman, Microscopy Research and Technique, 2005) for ImageJ (National Institutes of Health). Donor mTFP1 leakage was quantified using cells transfected with mini-Nesprin2G-mTFP1 alone, while acceptor Venus cross-excitation was quantified using cells transfected with mini-Nesprin2G-Venus alone. At least 10 cells each were used for bleed-through corrections. For FRET index determination, masks consisting of a 3 pixel-wide band encompassing the nuclear envelope were used to segment the nuclear envelope. Mean FRET index per nucleus was then determined using previously published software (MATLABR2014a, MathWorks, Kumar, et al. 2016 JCB).

Imaging of conformationally sensitive Lamin A/C was performed on a Leica SP5 confocal microscope using the LAS-AF software. LaminA/C (AF488) was imaged using a 488nm laser line (ex) and PMT detector set for AF488 emission; and the WGA (AF594) using a 594nm laser line (ex) and PMT detector set for AF594 emission. PMT gain was adjusted for each sample to avoid over/under exposure. Acquisition settings were standardized and maintained during experiments. Single plane images to determine the location of each cell within a colony were acquired using a 40x 1.25 NA air objective, imaging the AF488 and AF594 channels sequentially. Next, Z-stacks of each images were acquired using a 63x, 1.4 NA oil objective in the AF488 channel. Image zoom and size was adjusted such that voxel size was 55-65 nm in the xy-plane and 130 nm in the z-plane. Image stacks were deconvolved using Huygens Professional software (Scientific Volume Imaging, The Netherlands, http://svi.nl) as described (Ihalainen et al., 2015). A theoretical point spread function was used for iterative deconvolution. Deconvolution was performed using the following software parameters: image signal to noise

was set to 5, the quality threshold was 0.01, and maximum iterations was 50 (however usually fewer than 20 iterations were required to reach the quality threshold). Images were then analyzed using ImageJ (National Institutes of Health). The apical-basal Lamin A/C intensity was measured for a single XZ or YZ slice from the middle of each nuclei of interest. The intensity was measured using a straight line along the z-axis that is approximately half the width of the nucleus of interest. The fluorescence intensity across the z-axis was plotted and fit to two gaussian curves, the area under each curve and the ratio of these areas were calculated using MATLAB R2019b and the software can be found on GitHub at the following url: https://github.com/LusKingLab/GaussianFit.

RNAseq

WT and *Sun* dKO cells were grown in E-low calcium media for 24 h to 100% confluency (undifferentiated) or were switched to high calcium media to induce adhesion formation and differentiation for 48 h. Total RNA was isolated using the RNeasy Plus kit (QIAGEN) according to the manufacturer's instructions for three biological replicates for each condition. cDNA was synthesized using reagents from the TruSeq RNA sample preparation kit (Illumina) according to the manufacturer's instructions. cDNA libraries were sequenced (paired end 75 nts) at the Yale Stem Cell Center Genomics and Bioinformatics Core on the HiSeq4000 platform. Reads were mapped using BowTie/TopHat2 to the mm10 genome build. Differentially expressed genes between the WT and *Sun* dKO conditions in the undifferentiated and differentiated states were identified using DESeq2.

RT-qPCR

WT and *Sun* dKO keratinocytes were plated in a fibronectin-coated (50ng/mL; Sigma Aldrich) 6-well dish such that they were 70-80% confluent. They were cultured in E-low calcium media overnight before switching to 1.2 mM calcium media to induce differentiation for 48 hours. Total RNA was isolated using the RNeasy Plus kit (QIAGEN) according to the manufacturer's instructions. The iScript cDNA Synthesis Kit (BioRad) was used to generate cDNA from equal amounts of total RNA (1μg) according to the manufacturer's instructions. Quantitative real-time PCR was performed with a BioRad CFX96 using iTaq Universal SYBR Green Supermix (BioRad) for 40 cycles. Primers used include: GAPDH forward: AGGTCGGTGTGAACGGATTTG and reverse: TGTAGACCATGTAGTTGAGGTCA; Sprr1b forward: GATCCCAGCGACCACAC and reverse: GCTGATGTGAACTCATGCTTC. PCR product levels were normalized to GAPDH mRNA levels.

References:

Alam, S.G., Q. Zhang, N. Prasad, Y. Li, S. Chamala, R. Kuchibhotla, B. Kc, V. Aggarwal, S. Shrestha, A.L. Jones, S.E. Levy, K.J. Roux, J.A. Nickerson, and T.P. Lele. 2016. The mammalian LINC complex regulates genome transcriptional responses to substrate rigidity. *Sci Rep*. 6:38063.10.1038/srep38063

Chang, W., H.J. Worman, and G.G. Gundersen. 2015. Accessorizing and anchoring the LINC complex for multifunctionality. *J Cell Biol*. 208:11-22.10.1083/jcb.201409047

Connelly, J.T., J.E. Gautrot, B. Trappmann, D.W. Tan, G. Donati, W.T. Huck, and F.M. Watt. 2010. Actin and serum response factor transduce physical cues from the microenvironment to regulate epidermal stem cell fate decisions. *Nat Cell Biol*. 12:711-8.10.1038/ncb2074

Discher, D.E., D.J. Mooney, and P.W. Zandstra. 2009. Growth factors, matrices, and forces combine and control stem cells. *Science*. 324:1673-7.10.1126/science.1171643

Ezhkova, E., H. Pasolli, J. Parker, N. Stokes, I. Su, G. Hannon, A. Tarakhovsky, and E. Fuchs. 2009. Ezh2 orchestrates gene expression for the stepwise differentiation of tissue-specific stem cells. *Cell*. 136:1122-35

Gdula, M.R., K. Poterlowicz, A.N. Mardaryev, A.A. Sharov, Y. Peng, M.Y. Fessing, and V.A. Botchkarev. 2013. Remodeling of three-dimensional organization of the nucleus during terminal keratinocyte differentiation in the epidermis. *J Invest Dermatol*. 133:2191-201.10.1038/jid.2013.66

Grashoff, C., B.D. Hoffman, M.D. Brenner, R. Zhou, M. Parsons, M.T. Yang, M.A. McLean, S.G. Sligar, C.S. Chen, T. Ha, and M.A. Schwartz. 2010. Measuring mechanical tension across vinculin reveals regulation of focal adhesion dynamics. *Nature*. 466:263-6.10.1038/nature09198

Hotchin, N.A., A. Gandarillas, and F.M. Watt. 1995. Regulation of cell surface beta 1 integrin levels during keratinocyte terminal differentiation. *J Cell Biol*. 128:1209-19.10.1083/jcb.128.6.1209

Ihalainen, T.O., L. Aires, F.A. Herzog, R. Schwartlander, J. Moeller, and V. Vogel. 2015. Differential basal-to-apical accessibility of lamin A/C epitopes in the nuclear lamina regulated by changes in cytoskeletal tension. *Nat Mater*. 14:1252-61.10.1038/nmat4389

Jung, H.J., A. Tatar, Y. Tu, C. Nobumori, S.H. Yang, C.N. Goulbourne, H. Herrmann, L.G. Fong, and S.G. Young. 2014. An absence of nuclear lamins in keratinocytes leads to ichthyosis, defective epidermal barrier function, and intrusion of nuclear membranes and endoplasmic reticulum into the nuclear chromatin. *Mol Cell Biol*. 34:4534-44.10.1128/mcb.00997-14

Le, H.Q., S. Ghatak, C.Y. Yeung, F. Tellkamp, C. Günschmann, C. Dieterich, A. Yeroslaviz, B. Habermann, A. Pombo, C.M. Niessen, and S.A. Wickström. 2016. Mechanical regulation of transcription controls Polycomb-mediated gene silencing during lineage commitment. *Nat Cell Biol*. 18:864-75.10.1038/ncb3387

Levy, L., S. Broad, D. Diekmann, R.D. Evans, and F.M. Watt. 2000. beta1 integrins regulate keratinocyte adhesion and differentiation by distinct mechanisms. *Mol Biol Cell*. 11:453-66

Lien, W.H., X. Guo, L. Polak, L.N. Lawton, R.A. Young, D. Zheng, and E. Fuchs. 2011. Genome-wide maps of histone modifications unwind in vivo chromatin states of the hair follicle lineage. *Cell Stem Cell*. 9:219-32.10.1016/j.stem.2011.07.015

Luxton, G.W., E.R. Gomes, E.S. Folker, H.J. Worman, and G.G. Gundersen. 2011. TAN lines: a novel nuclear envelope structure involved in nuclear positioning. *Nucleus*. 2:173-81.10.4161/nucl.2.3.16243

Mardaryev, A.N., M.R. Gdula, J.L. Yarker, V.U. Emelianov, V.N. Emelianov, K. Poterlowicz, A.A. Sharov, T.Y. Sharova, J.A. Scarpa, B. Joffe, I. Solovei, P. Chambon, V.A. Botchkarev,

and M.Y. Fessing. 2014. p63 and Brg1 control developmentally regulated higher-order chromatin remodelling at the epidermal differentiation complex locus in epidermal progenitor cells. *Development*. 141:101-11.10.1242/dev.103200

Mertz, A.F., Y. Che, S. Banerjee, J.M. Goldstein, K.A. Rosowski, S.F. Revilla, C.M. Niessen, M.C. Marchetti, E.R. Dufresne, and V. Horsley. 2013. Cadherin-based intercellular adhesions organize epithelial cell-matrix traction forces. *Proc Natl Acad Sci U S A*. 110:842-7.10.1073/pnas.1217279110

Oh, I.Y., D.M. Albea, Z.A. Goodwin, A.M. Quiggle, B.P. Baker, A.M. Guggisberg, J.H. Geahlen, G.M. Kroner, and C.d.G. Strong. 2014. Regulation of the Dynamic Chromatin Architecture of the Epidermal Differentiation Complex Is Mediated by a c-Jun|[sol]|AP-1-Modulated Enhancer. *Journal of Investigative Dermatology*. 134:2371-2380.doi:10.1038/jid.2014.44

Raghavan, S., C. Bauer, G. Mundschau, Q. Li, and E. Fuchs. 2000. Conditional ablation of beta1 integrin in skin. Severe defects in epidermal proliferation, basement membrane formation, and hair follicle invagination. *J Cell Biol*. 150:1149-60

Rippa, A.L., E.A. Vorotelyak, A.V. Vasiliev, and V.V. Terskikh. 2013. The role of integrins in the development and homeostasis of the epidermis and skin appendages. *Acta Naturae*. 5:22-33

Stewart, R.M., A.E. Zubek, K.A. Rosowski, S.M. Schreiner, V. Horsley, and M.C. King. 2015. Nuclear-cytoskeletal linkages facilitate cross talk between the nucleus and intercellular adhesions. *J Cell Biol*. 209:403-18.10.1083/jcb.201502024

Tajik, A., Y. Zhang, F. Wei, J. Sun, Q. Jia, W. Zhou, R. Singh, N. Khanna, A.S. Belmont, and N. Wang. 2016. Transcription upregulation via force-induced direct stretching of chromatin. *Nat Mater*. 15:1287-1296.10.1038/nmat4729

Totaro, A., T. Panciera, and S. Piccolo. 2018. YAP/TAZ upstream signals and downstream responses. *Nat Cell Biol*. 20:888-899.10.1038/s41556-018-0142-z

Tsuruta, D., T. Hashimoto, K.J. Hamill, and J.C. Jones. 2011. Hemidesmosomes and focal contact proteins: functions and cross-talk in keratinocytes, bullous diseases and wound healing. *J Dermatol Sci*. 62:1-7.10.1016/j.jdermsci.2011.01.005

Wang, N., J.D. Tytell, and D.E. Ingber. 2009. Mechanotransduction at a distance: mechanically coupling the extracellular matrix with the nucleus. *Nat Rev Mol Cell Biol*. 10:75-82.10.1038/nrm2594

Watt, F.M., M.D. Kubler, N.A. Hotchin, L.J. Nicholson, and J.C. Adams. 1993. Regulation of keratinocyte terminal differentiation by integrin-extracellular matrix interactions. *J Cell Sci*. 106 (Pt 1):175-82

Williams, R.R.E., S. Broad, D. Sheer, and J. Ragoussis. 2002. Subchromosomal positioning of the epidermal differentiation complex (EDC) in keratinocyte and lymphoblast interphase nuclei. *Experimental Cell Research*. 272:163-175.10.1006/excr.2001.5400

Zhang, X., K. Lei, X. Yuan, X. Wu, Y. Zhuang, T. Xu, R. Xu, and M. Han. 2009. SUN1/2 and Syne/Nesprin-1/2 complexes connect centrosome to the nucleus during neurogenesis and neuronal migration in mice. *Neuron*. 64:173-87.10.1016/j.neuron.2009.08.018

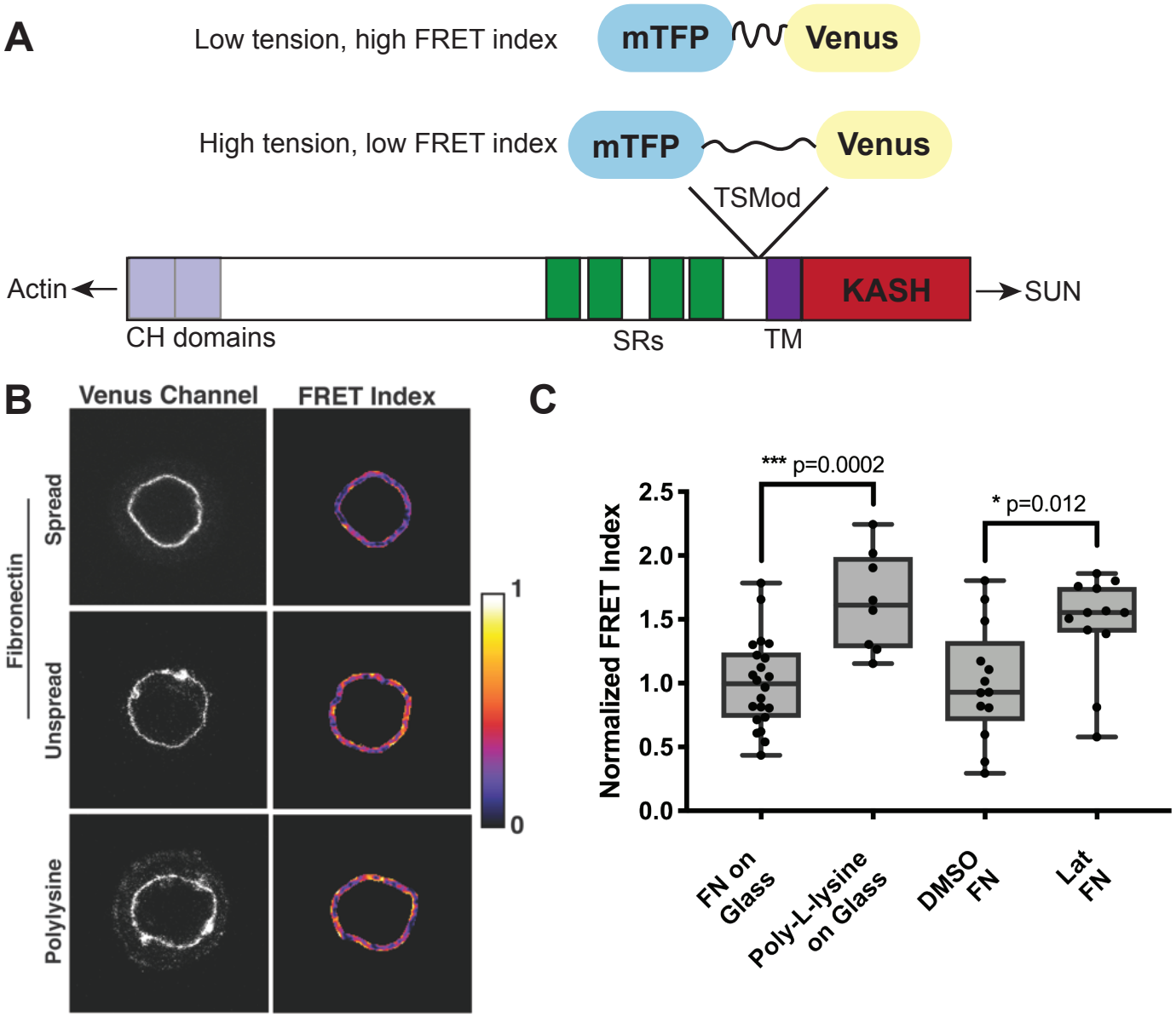
A
Low tension, high FRET index
mTFP
Venus
High tension, low FRET index
mTFP
Venus
TSMod
Actin
KASH
SUN
CH domains
SRs
TM
B
Venus Channel
FRET Index
Fibronectin
Spread
Unspread
Polylysine
1
0
C
*** p=0.0002
* p=0.012
Normalized FRET Index
2.5
2.0
1.5
1.0
0.5
0.0
FN on Glass
Poly-L-lysine on Glass
DMSO FN
Lat FN

Figure 1

Figure 1

A tension sensor in mini-Nesprin2 is under actin-dependent tension when WT mouse keratinocytes are plated on fibronectin-coated substrates. (A) Cartoon of the N2G-JM-TSMod, in which the mTFP-Venus tension sensor module is inserted between the cytoplasmic domain and the C-terminal KASH domain/transmembrane domain. Tension leads to a reduction in the FRET index. **(B)** At low expression levels the N2G-JM-TSMod is targeted efficiently to the nuclear envelope when plated on poly-lysine or fibronectin. Tension on the N2G-JM-TSMod is lowest in mouse keratinocytes after being fully spread on fibronectin, as indicated by the lower FRET index. **(C)** Tension on the N2G-JM-TSMod is higher in response to plating on fibronectin compared to poly-lysine and requires an intact actin network as revealed by latrunculin (LAT) treatment. Statistical significance determined by unpaired t-test.

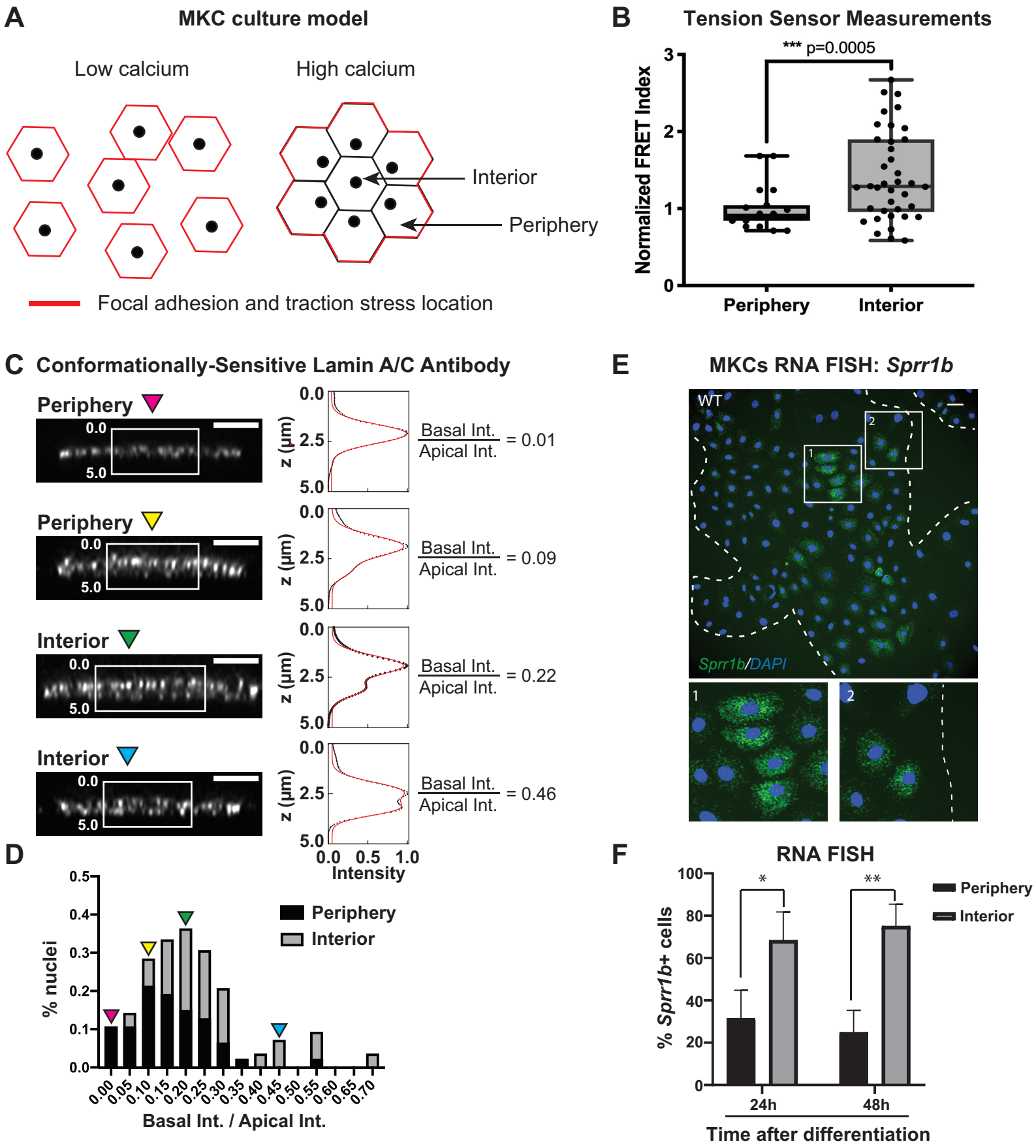
A
MKC culture model
Low calcium
High calcium
Interior
Periphery
Focal adhesion and traction stress location
B
Tension Sensor Measurements
*** p=0.0005
Normalized FRET Index
Periphery
Interior
C
Conformationally-Sensitive Lamin A/C Antibody
Periphery
Periphery
Interior
Interior
z (µm)
Intensity
Basal Int. / Apical Int. = 0.01
Basal Int. / Apical Int. = 0.09
Basal Int. / Apical Int. = 0.22
Basal Int. / Apical Int. = 0.46
D
% nuclei
Periphery
Interior
Basal Int. / Apical Int.
E
MKCs RNA FISH: Sprr1b
WT
Sprr1b/DAPI
F
RNA FISH
% Sprr1b+ cells
Periphery
Interior
24h
48h
Time after differentiation

Figure 2

Figure 2

Tension on the N2G-JM-TSMod and nuclear lamina is released at the interior of cohesive mouse keratinocyte (MKC) colonies concomitant with differentiation. (A) Cartoon of cell junction reorganization upon differentiation. In single MKCs grown in low calcium media focal adhesions and traction forces are found at the periphery of each cell (red). In response to high calcium, MKCs form cohesive colonies and engage cell-cell junctions, which leads to a reorganization of focal adhesions and traction forces to the colony periphery. Cells in the colony interior have cell-cell but not cell-matrix adhesions. **(B)** The FRET index is higher in cells at the interior of cohesive MKC colonies compared to cells at the periphery, suggesting that tension on the N2G-JM-TSMod requires cell-intrinsic focal adhesion engagement. **(C)** Staining of cohesive MKC colonies by immunofluorescence using a conformationally-sensitive lamin A/C antibody reveals that tension on the basal nuclear surface is relaxed at the colony interior relative to the colony periphery. Examples of xz and yz confocal sections and corresponding Z-intensity profiles measured in the region indicated by the white box (left). Intensity profiles were fit to two gaussians (right). The intensity of antibody staining was defined as the area under the curve of the gaussian distribution corresponding to each side of the nuclear envelope and a ratio of the intensity of antibody staining of the basal relative to the apical side of the nuclear envelope was calculated. Scale bar = 5 μm. **(D)** A histogram of the ratio of basal to apical intensity calculated as described in (C) for all cells analyzed (n = 47 for periphery and n = 28 for interior) shows that the ratio of basal to apical intensity for interior cells is shifted to higher values relative to cells at the periphery, indicating the lamina is under less tension. Values were binned every 0.05 arbitrary units and the central value of each bin is labeled. Representative images for the low (magenta triangle) and high (blue triangle) bins, and bins corresponding to the highest percentage of periphery (yellow triangle) and interior (green triangle) are shown in (C). **(E-F)** The differentiation marker Sprr1b is expressed at higher levels in the colony interior than at the colony periphery. **(E)** Representative image of RNA FISH for Sprr1b 24 hours after addition of calcium to induce differentiation. Inset 1 shows Sprr1b positive cells at the colony interior. Inset 2 shows Sprr1b positive cells at the colony periphery. Dotted lines are colony outline. Scale bar = 100 μm. **(F)** Quantitation of the percent of Sprr1b positive cells that are located at the interior and periphery of WT MKC colonies normalized to the total Sprr1b positive cells. 24h = 24 hours calcium treatment. 48h = 48 hours calcium treatment. * p value < 0.05. ** p value <0.01 as determined by unpaired t-test. Error bars are SD. N = 3 biological replicates.

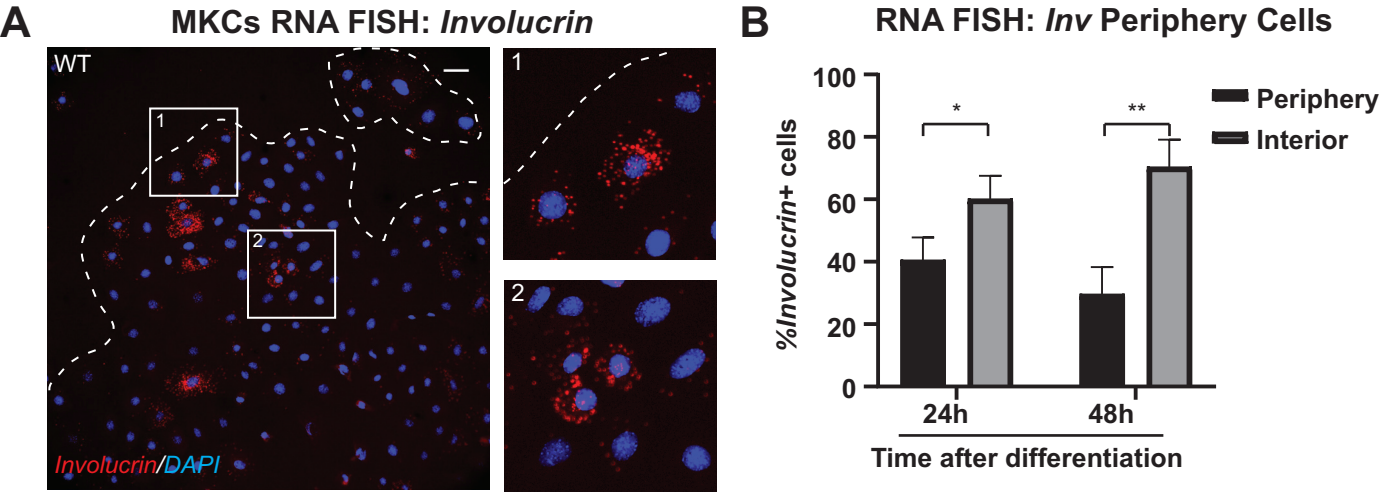

Figure 2-figure supplement 1

Figure 2-figure supplement 1

(A-B) The differentiation marker involucrin is expressed at higher levels in the colony interior than at the colony periphery. **(A)** Representative image of RNA FISH for involucrin 24 hours after addition of calcium to induce differentiation. Inset 1 shows Sprr1b positive cells at the colony interior. Inset 2 shows Sprr1b positive cells at the colony periphery. Dotted lines are colony outline. Scale bar = 100 μm. **(B)** Quantitation of the percent of involucrin positive cells that are located at the interior and periphery of WT MKC colonies normalized to the total Sprr1b positive cells. 24h = 24 hours calcium treatment. 48h = 48 hours calcium treatment. Unpaired t-test was done to determine statistical significance. * p value < 0.05. ** p value <0.01. Error bars are SD. N = 3 biological replicates.

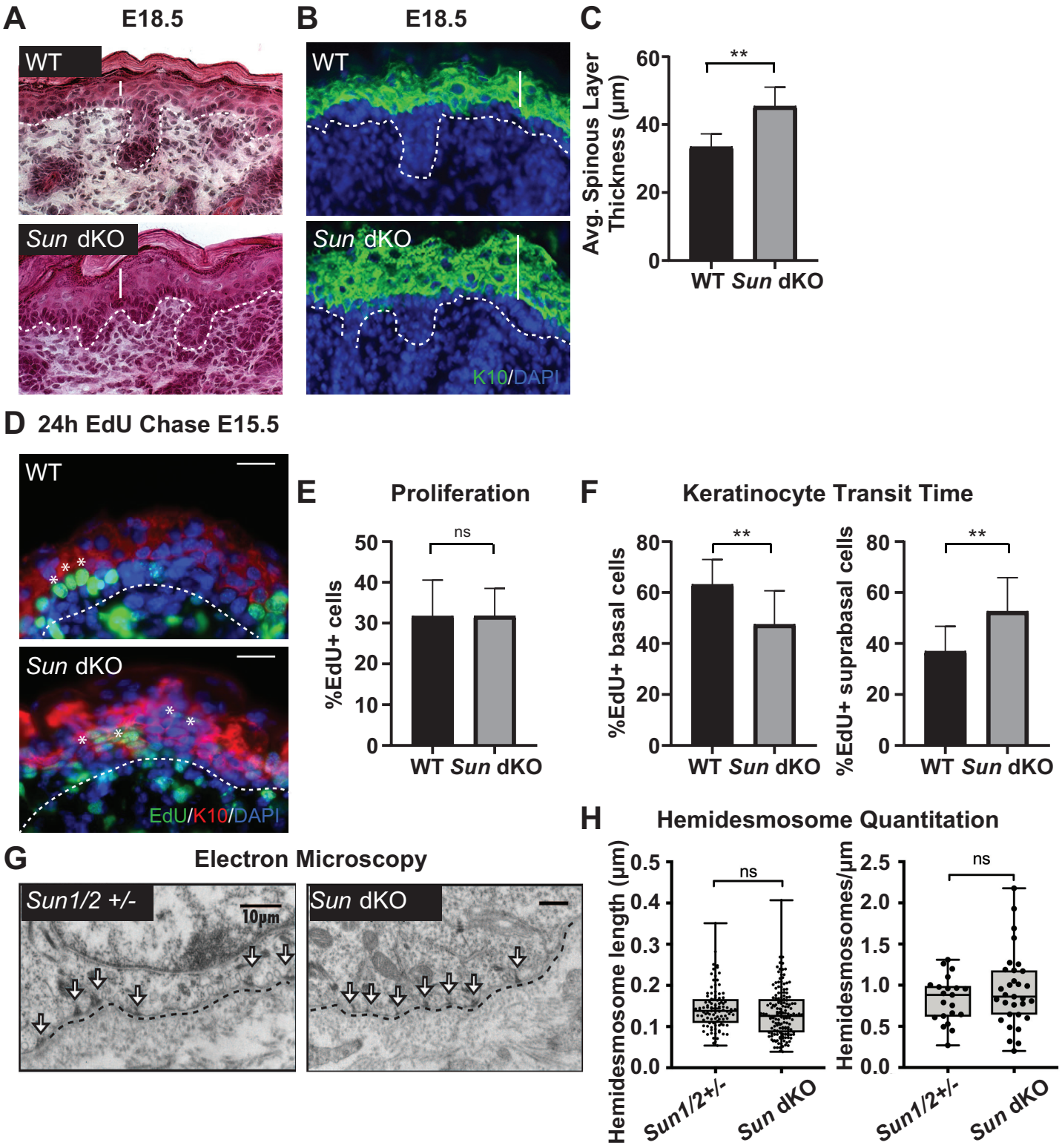
A
E18.5
WT
Sun dKO
B
E18.5
WT
Sun dKO
K10/DAPI
C
Avg. Spinous Layer Thickness (µm)
60
40
20
0
**
WT Sun dKO
D 24h EdU Chase E15.5
WT
Sun dKO
EdU/K10/DAPI
E
Proliferation
%EdU+ cells
50
40
30
20
10
0
ns
WT Sun dKO
F
Keratinocyte Transit Time
%EdU+ basal cells
80
60
40
20
0
**
WT Sun dKO
%EdU+ suprabasal cells
80
60
40
20
0
**
WT Sun dKO
G
Electron Microscopy
Sun1/2 +/-
10µm
Sun dKO
H
Hemidesmosome Quantitation
Hemidesmosome length (µm)
0.5
0.4
0.3
0.2
0.1
0.0
ns
Sun1/2+/-
Sun dKO
Hemidesmosomes/µm
2.5
2.0
1.5
1.0
0.5
0.0
ns
Sun1/2+/-
Sun dKO

Figure 3

Figure 3

LINC complex ablation leads to precocious epidermal differentiation *in vivo*. (A) Increased epidermal thickness in *Sun* dKO mice. Representative Hematoxylin and Eosin staining of WT and *Sun* dKO skin at age E18.5. Dotted line denotes dermal/epidermal junction. Vertical line denotes epidermal thickness. **(B)** Expansion of the spinous layer in *Sun* dKO mice. Representative immunostaining for keratin 10 (K10) in WT and *Sun* dKO skin at age E15.5. Dotted line denotes dermal/epidermal junction. Vertical line denotes spinous layer thickness. Nuclei are stained with DAPI. **(C)** Quantitation of average spinous layer thickness as determined by immunostaining for K10 in WT and *Sun* dKO epidermis at E15.5. Unpaired t-test was used to determine statistical significance. ** p value <0.01. Error bars are SD. N = 5-8 biological replicates per genotype. **(D-F)** Pulse chase analysis reveals ab increase in EdU-positive cells in the suprabasal layers of *Sun* dKO mice (and decrease in EdU-positive basal cells) but no increase in overall proliferation. **(D)** Representative images of E15.5 WT and *Sun* dKO skin 24 hours after EdU pulse. Spinous layer keratinocytes are marked by K10 staining. Dotted line denotes dermal/epidermal junction. Asterisks denote suprabasal keratinocytes marked with EdU. Scale bar = 20 μM. Nuclei are stained with DAPI. **(E)** Quantitation of total EdU positive cells normalized to total epidermal cells in both WT and *Sun* dKO epidermis at E15.5. Statistical significance was determined using unpaired t-test. Ns = not significant. N = 3 mice/genotype. **(F)** Quantitation of location of EdU positive cells in the epidermis of E15.5 WT and *Sun* dKO epidermis 24 hours after EdU pulse. K10 staining was used to differentiation suprabasal from basal keratinocytes. Statistical significance was determined by performing unpaired t-test. ** p value < 0.01. N = 3 mice/genotype. **(G-H)** Adhesion between basal keratinocytes and the basal lamina is normal in the *Sun* dKO skin. **(G)** Representative electron microscopy images of P0.5 WT and *Sun* dKO basal keratinocytes in vivo. Scale bar = 10 μm. Dotted line denotes basement membrane. Arrows point to hemidesmosomes. **(H)** Quantitation of hemidesmosome length (left) and the number of hemidesmosomes per surface area (right) in control and *Sun* dKO epidermis at age P0.5. ns = not statistically significant as determined by unpaired t-test.

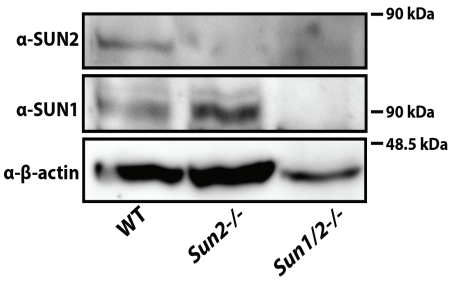

Figure 3-figure supplement 1

Figure 3-figure supplement 1
Western blots analysis of WT, *Sun2* -/- and *Sun* dKO primary keratinocytes for the proteins SUN1 and SUN2. β-actin was used as a loading control.

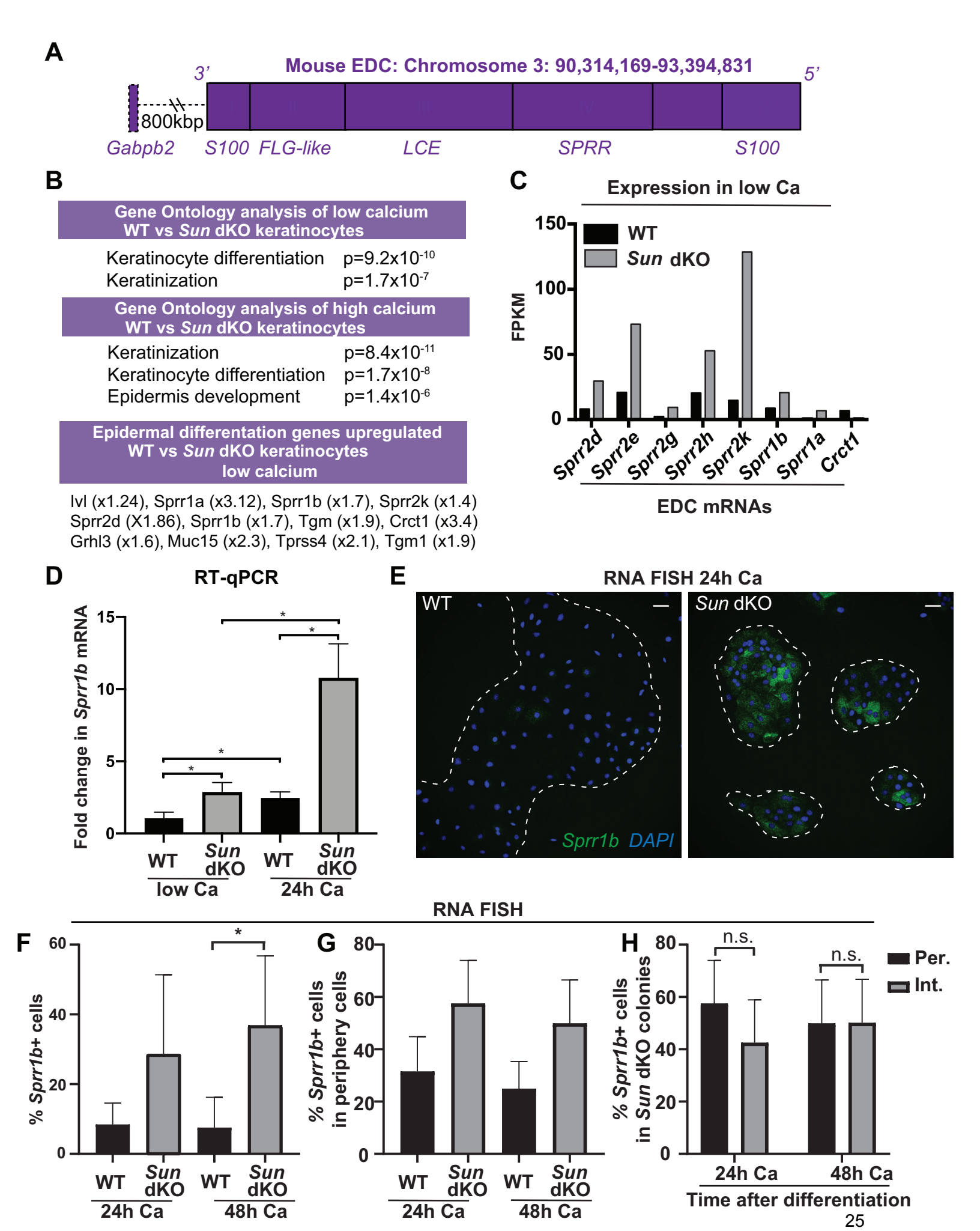
A
Mouse EDC: Chromosome 3: 90,314,169-93,394,831
3'
5'
800kbp
Gabpb2
S100
FLG-like
LCE
SPRR
S100
B
Gene Ontology analysis of low calcium WT vs Sun dKO keratinocytes
Keratinocyte differentiation p=9.2x10-10
Keratinization p=1.7x10-7
Gene Ontology analysis of high calcium WT vs Sun dKO keratinocytes
Keratinization p=8.4x10-11
Keratinocyte differentiation p=1.7x10-8
Epidermis development p=1.4x10-6
Epidermal differentation genes upregulated WT vs Sun dKO keratinocytes low calcium
lvl (x1.24), Sprr1a (x3.12), Sprr1b (x1.7), Sprr2k (x1.4)
Sprr2d (X1.86), Sprr1b (x1.7), Tgm (x1.9), Crct1 (x3.4)
Grhl3 (x1.6), Muc15 (x2.3), Tprss4 (x2.1), Tgm1 (x1.9)
C
Expression in low Ca
WT
Sun dKO
FPKM
150
100
50
0
Sprr2d
Sprr2e
Sprr2g
Sprr2h
Sprr2k
Sprr1b
Sprr1a
Crct1
EDC mRNAs
D
RT-qPCR
Fold change in Sprr1b mRNA
15
10
5
0
WT
Sun dKO
WT
Sun dKO
low Ca
24h Ca
E
RNA FISH 24h Ca
WT
Sun dKO
Sprr1b DAPI
RNA FISH
F
% Sprr1b+ cells
60
40
20
0
WT
Sun dKO
WT
Sun dKO
24h Ca
48h Ca
G
% Sprr1b+ cells in periphery cells
80
60
40
20
0
WT
Sun dKO
WT
Sun dKO
24h Ca
48h Ca
H
% Sprr1b+ cells in Sun dKO colonies
80
60
40
20
0
n.s.
n.s.
Per.
Int.
24h Ca
48h Ca
Time after differentiation

Figure 4

Figure 4

LINC complex ablation leads to precocious MKC differentiation in vivo, which is associated with aberrant up-regulation of differentiation markers at the colony periphery. (A) Cartoon of the epidermal differentiation complex (EDC), a large genic region that is coordinately up-regulated upon epidermal differentiation. **(B)** Comparative transcriptome analysis reveals that *Sun* dKO MKCs display precocious expression of epidermal differentiation genes when cultured in low calcium media and higher levels of expression of epidermal differentiation genes in high calcium media. **(C)** Examples of EDC genes that are precociously expressed in *Sun* dKO MKCs cultured in low calcium media from the RNAseq data, expressed as fragments per kb of transcript per million reads. **(D)** Real-time qPCR analysis of Sprr1b in WT and *c* in the presence and absence of calcium validates precocious Sprr1b expression in *Sun* dKO cells without calcium stimulation. Ct values were normalized to GAPDH. Fold change in expression was determined by calculating the $2^{\Delta\Delta Ct}$ relative to the mean of WT no calcium ΔCt. n=3 biological replicates for all conditions. Statistical significance was determined by performing multiple t-tests. * = $p < 0.05$. The Holm-Sidak method was used to correct for multiple comparisons. Error bars are SD. N = 3 biological replicates. **(E - G)** Cohesive *Sun* dKO MKCs express elevated levels of differentiation markers and lose the relationship between position in the colony and EDC gene expression. **(E)** Quantitation of RNA FISH for Sprr1b in WT and *Sun* dKO MKCs after calcium treatment. Sprr1b positive cells were counted and normalized to total cells in each field. 24h = 24 hours calcium treatment. 48h = 48 hours calcium treatment. Statistical significance was determined by performing unpaired t-test. * p value < 0.05. Error bars are SD. N = 3 biological replicates. **(F)** Representative images of RNA FISH for Sprr1b in WT and *Sun* dKO MKCs after 24 hours calcium treatment. Dotted lines are colony outline. Scale bar = 100 µm. **(G)** Quantitation of the percent Sprr1b positive cells that are located at the periphery of WT and *Sun* dKO MKC colonies normalized to the total Sprr1b positive cells. 24h Ca = 24 hours calcium treatment. 48h Ca = 48 hours calcium treatment. Error bars are SD. N = 3 biological replicates.

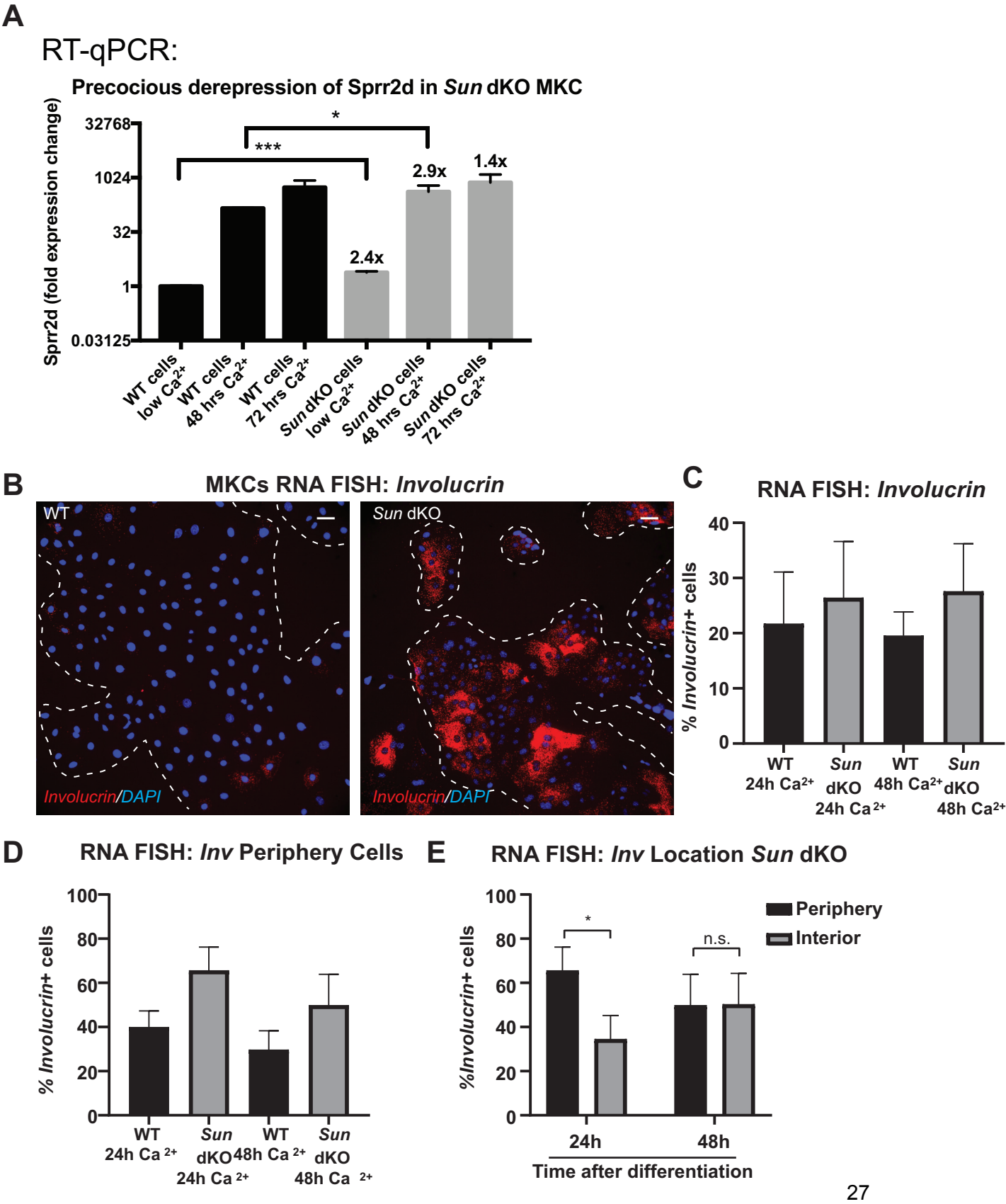

Figure 4-figure supplement 1

Figure 4-figure supplement 1

(A) Real-time qPCR demonstrating precocious expression of Sprr2b in Sun dKO cells. **(B)** Representative images of RNA FISH for involucrin in WT and *Sun* dKO MKCs after 24 hours calcium treatment. Dotted lines are colony outline. Scale bar = 100 µm. **(C)** Quantitation of RNA FISH for involucrin in WT and *Sun* dKO MKCs after calcium treatment. Involucrin positive cells were counted and normalized to total cells in each field. 24h = 24 hours calcium treatment. 48h = 48 hours calcium treatment. Error bars are SD. N = 3 biological replicates. **(D)** Quantitation of the percent involucrin positive cells that are located at the periphery of WT and *Sun* dKO MKC colonies normalized to the total involucrin positive cells. 24h Ca = 24 hours calcium treatment. 48h Ca = 48 hours calcium treatment. Error bars are SD. N = 3 biological replicates. **(E)** After 48 hours *Sun* dKO MKCs fail to display a bias in involucrin express towards the colony interior (as seen in WT MKCs (Fig. 2-figure supplement 1B).

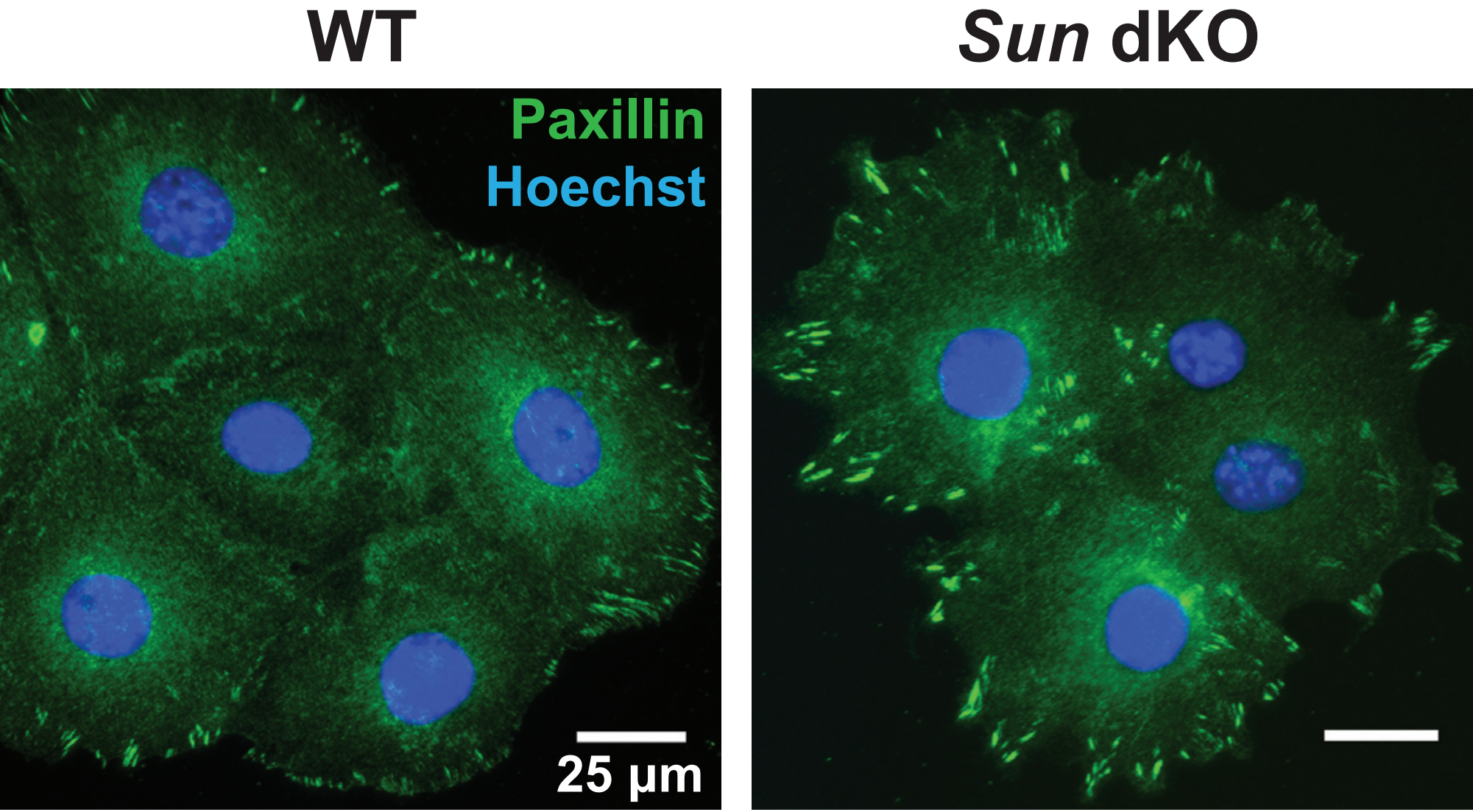

Figure 4-figure supplement 2

Figure 4-figure supplement 2
Cohesive *Sun* dKO MKC colonies have focal adhesions at the colony periphery. WT and *Sun* dKO MKCs were cultured in calcium for 48 hours and stained with anti-paxillin antibodies and Hoechst.

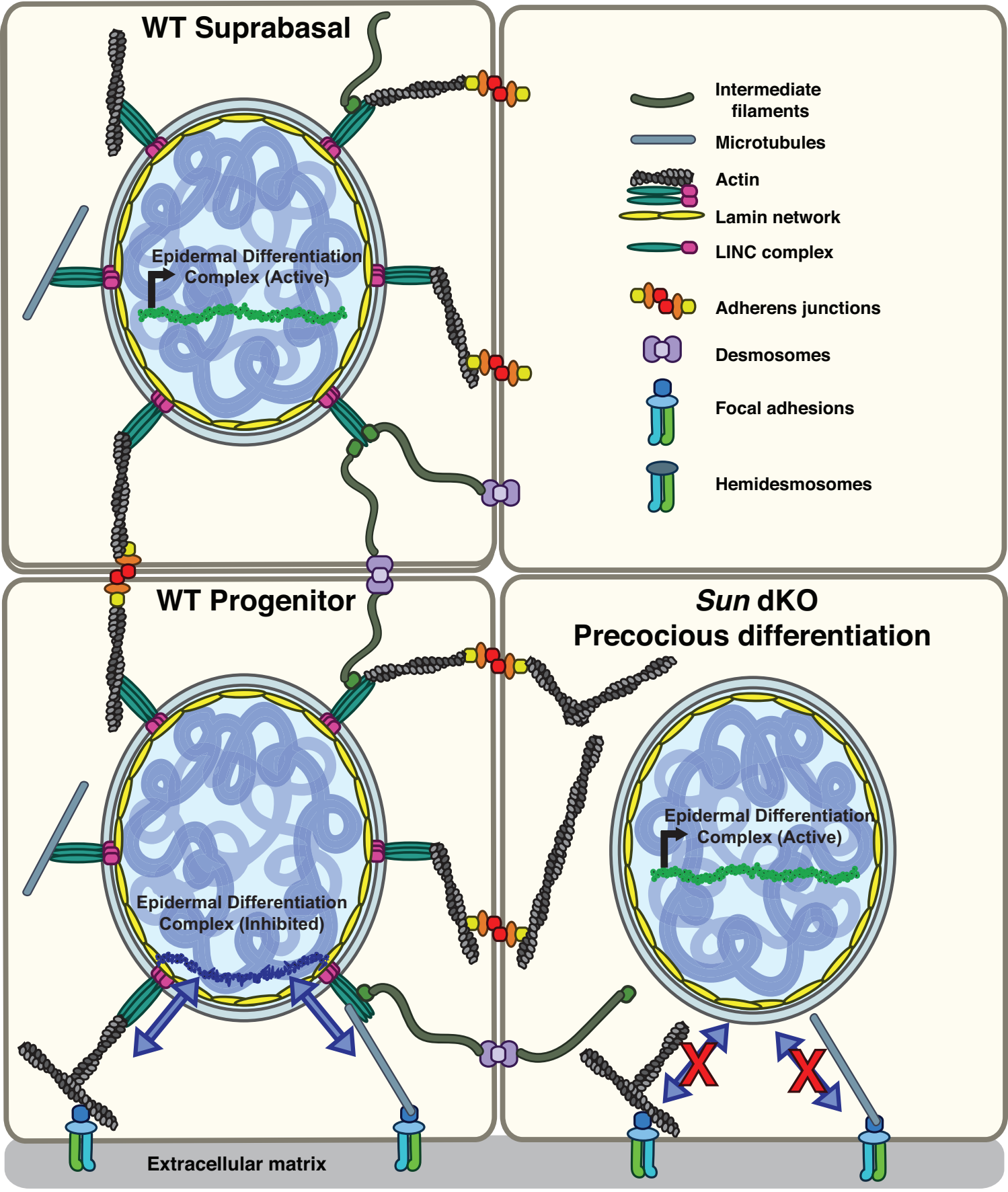
WT Suprabasal
Epidermal Differentiation Complex (Active)
Intermediate filaments
Microtubules
Actin
Lamin network
LINC complex
Adherens junctions
Desmosomes
Focal adhesions
Hemidesmosomes
WT Progenitor
Epidermal Differentiation Complex (Inhibited)
Sun dKO
Precocious differentiation
Epidermal Differentiation Complex (Active)
Extracellular matrix

Figure 5

Figure 5.
Model for the mechanism of precocious differentiation in *Sun* dKO epidermis. WT progenitor cells adhere to the basal lamina through integrins, leading to tension on LINC complexes that is transmitted to the basal surface of the nuclear lamina to maintain repression of the EDC. As cells move into the suprabasal layer they lose integrin engagement. In suprabasal cells that only engage cell-cell junctions LINC complexes and the nuclear lamina are relaxed, leading to up-regulation of EDC gene expression. In the *Sun* dKO epidermis, tension from engaged integrins is not propagated to the nucleus in progenitor cells despite normal adhesion, leading to precocious expression of EDC genes.